Materials Research Express

PAPER • OPEN ACCESS

Computational exploration of biomedical HfNbTaTiZr and $Hf_{0.5}Nb_{0.5}Ta_{0.5}Ti_{1.5}Zr$ refractory high-entropy alloys

Materials Research Express

PAPER

Computational exploration of biomedical HfNbTaTiZr and $Hf_{0.5}Nb_{0.5}Ta_{0.5}Ti_{1.5}Zr$ refractory high-entropy alloys

Uttam Bhandari[1], **Hamed Ghadimi**[1], **Congyan Zhang**[2], **Feng Gao**[3], **Shizhong Yang**[2] **and Shengmin Guo**[1]

[1] Department of Mechanical and Industrial Engineering, Louisiana State University, Baton Rouge, United States of America
[2] Department of Computer Science, Southern University and A&M College, Baton Rouge, United States of America
[3] Department of Mathematics and Physics, Southern University and A&M College, Baton Rouge, United States of America

E-mail: feng.gao@sus.edu

Keywords: refractory high entropy alloys, HfNbTaTiZr, density functional theory, supercell, thermal properties

OPEN ACCESS

RECEIVED
13 July 2021

REVISED
4 August 2021

ACCEPTED FOR PUBLICATION
13 August 2021

PUBLISHED
30 September 2021

Abstract

Refractory high entropy alloys (RHEAs) have been proven to be a potential candidate in the biomedical field due to their balanced mechanical properties and biocompatible composition. Recent experimental findings show that RHEAs like HfNbTaTiZr and $Hf_{0.5}Nb_{0.5}Ta_{0.5}Ti_{1.5}Zr$ have good mechanical properties such as high polarization and wear resistance than others which establish them as potential materials for biomedical application. In this work, we performed first-principles density functional theory calculations on the mechanical and thermal properties of HfNbTaTiZr and $Hf_{0.5}Nb_{0.5}Ta_{0.5}Ti_{1.5}Zr$. The predicted lattice constant, density, Young's modulus, and Vickers hardness are consistent with the available experimental report, which verifies the accuracy of the applied model. The thermal coefficient of linear expansion of both RHEAs has been investigated by utilizing the Debye theory. The present methods could be applied to study other future RHEAs on exploration of their physical properties.

1. Introduction

The use of biomaterials in implantation has attracted the interest of researchers in the biomedical field due to their attractive physical properties such as high strength, biocompatibility, corrosion resistance, and wear resistance [1–4]. The commonly used biomedical alloys includes 316L, stainless steel, CoCrMo, Ti6Al4V, and titanium-based alloys [5–9]. However, these materials are very sensitive to body fluids, which can easily corrode and release toxic metallic ions (Ni, Cr, Co and Al) when used for a long term [7, 10–14]. For example, titanium alloy, Ti6Al4V is promising and is widely used for implant applications, but it releases ions of V and Al which affects the organs and tissues of patient's body. Recent study shows the aluminum ions is a possible cause for Alzheimer disease, while vanadium oxide is a toxic chemical for human body [15–17]. This results in early failure of the implants system which is not desirable. The demand for implants is increasing in developed countries to maintain the quality of life of aged people. Therefore, it is necessary to design metallic alloys with balanced mechanical properties, high hardness, high corrosion resistance, and biocompatibility [18, 19].

Refractory high entropy alloys (RHEAs) are advanced novel class metallic alloys that are comprised of five or more different elements, each element has a concentration ranging from 5 to 35 at.% [20, 21]. As compared to traditional metallic alloys, RHEAs consist of alloying refractory elements such as titanium (Ti), zirconium (Zr), molybdenum (Mo), niobium (Nb), iron (Fe), vanadium (V), and tantalum (Ta). RHEAs are considered to be favorable refractory alloys with non-allergic and non-toxic properties [22–25]. Therefore, compared to traditional metallic alloys, they have great potential application in biomedical field [26].

HfNbTaTiZr was extensively studied for high temperature application in the past [27–32]. Recently Amir *et al* [33] synthesized equimolar HfNbTaTiZr and non-equimolar $Hf_{0.5}Nb_{0.5}Ta_{0.5}Ti_{1.5}Zr$ RHEAs by arc melting method and investigated their microstructure, mechanical, corrosion and wettability properties for possible biomedical application. They compared the properties of two RHEAs, HfNbTaTiZr and $Hf_{0.5}Nb_{0.5}Ta_{0.5}Ti_{1.5}Zr$, with 316L, CoCrMo, and Ti6Al4V alloys. The two studied RHEAs showed greater polarization and wear

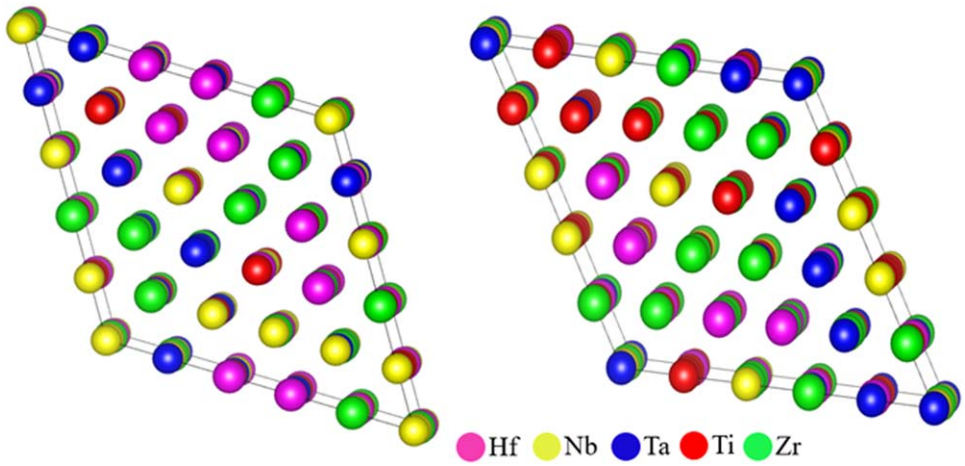

Figure 1. 100 atoms supercell model with randomly distributed elements. The left-hand side figure represents the supercell of HfNbTaTiZr whereas the right-hand side figure represents the supercell of $Hf_{0.5}Nb_{0.5}Ta_{0.5}Ti_{1.5}Zr$.

resistance than CoCrMo, 316L, and Ti6Al4V. Both RHEAs exist in BCC stable phase with lattice constant of 3.249 A and 3.405 A, respectively. These two RHEAs are composed of purely biocompatible elements and show promising characteristics for biomedical applications. Many experiments have been conducted regarding the design and characterization of RHEAs for biomedical applications [34–40]. However, most experimental studies focus on the structural and mechanical properties with limited study on other thermodynamics properties. For the real application of RHEAs, detailed investigation of electronic, structural, mechanical, and thermodynamic properties is very important. Moreover, computational methods are economical and easier to investigate the alloys' structural, mechanical, and thermal properties as compared to experimental techniques.

In this report, the comparative study of electronic, mechanical, and thermodynamics properties of two RHEAs, HfNbTaTiZr and $Hf_{0.5}Nb_{0.5}Ta_{0.5}Ti_{1.5}Zr$, are performed by using first-principles density functional theory (DFT) calculations. The accuracy of the predicted properties of both RHEAs was further validated by comparing with available experimental data. It has been observed that the calculated mechanical properties are in good agreement with the available experiments. The quasi-harmonic Debye-Grüneisen theory was adopted to compute the thermodynamics properties.

2. Computational method

All mechanical properties were calculated using Vienna *Ab-Initio* Simulation Package (VASP) 5.4 [41] in MedeA software [42]. The generalized gradient approximation (GGA) [43] of Perdew-Burke-Ernzerhof (PBE) [44] is used as an exchange-correlation function. The plane wave cut off 500 eV was used in all calculations. The convergence criterion is 0.02 eV/Ang. The electronic iterations convergence is 10^{-5} eV using the blocked Davidson algorithm. The applied k-spacing of 0.2 per Angstrom, leads to a $4 \times 3 \times 3$ mesh in our calculation. This gives a k-spacings of $0.185 \times 0.197 \times 0.197$ per Angstrom. The first order Methfessel-Paxton smearing with a width of 0.2 eV was used. A first-principles calculation is performed to predict the mechanical properties of RHEAs. Previously, this method has been successfully applied for studying the alloying effects of element on structural, mechanical, and thermal properties of RHEAs [45–48]. Hu *et al* [45] studied the hydrogen behaviors and microstructural development in the HEA TiZrHfMoNb by applying first-principles method.

The random structure of BCC supercell is constructed by utilizing the python code and Knuth shuffle model [49] consisting of 100 atoms and is shown in figure 1. Virtual crystal approximation (VCA) [50] and special quasi-random structure (SQS) [51] are often used methods for simulating random distribution of RHEAs components on a given crystal lattice. However, VCA methods do not consider the effect of lattice distortion that exists in complex RHEAs whereas the SQS method considers the lattice distortion effect by combining the idea of cluster expansion with large supercells [52]. For complex RHEAs, large supercells are required to resemble the random distribution of elements. As an example, Tian *et al* [53] have constructed a large supercell of 250 and 128 atoms using the Alloy Theoretic Automated Toolkit to study the elastic properties of various RHEAs. The major limiting factor of the SQS model is the high computational cost associated with a large supercell. The proposed 100 atoms random supercell model is capable of distributing the components of the complex alloy randomly and its convergence test has been succinctly described in a previous publication [54]. This 100 atoms supercell is appropriate for providing highly accurate results with low computational costs.

The stress-strain method [55, 56] which is implemented in MedeA software is used to calculate the elastic constants C_{11}, C_{12}, and C_{44}. VASP computes the stress tensor by applying analytic expressions. Several strains are used to get more points for the fitting procedure involved in the calculation of the elastic constants. The equilibrium supercell is optimized with high accuracy to avoid zero strain. The Voight-Reuss-Hill approximation [57] was used to calculate bulk modulus (B), Shear modulus (G), Young's modulus (E), and Poisson ratio (ν).

The formula to compute B, G, E, and ν are

$$B = \frac{1}{3}(C_{11} + 2C_{12}),\ G = \frac{1}{2}(G_{Voight} + G_{Reuss}),$$

where

$$G_{Voight} = \frac{1}{5}(C_{11} - C_{12} + 3C_{44})$$

and

$$G_{Reuss} = \frac{5}{4(S_{11} - S_{12}) + 3S_{44}},$$

S is compliance matrix,

$$E = 9BG/3B + G \text{ and } \nu = 3B - 2G/2(3B + G). \tag{1}$$

The Grüneisen-Debye approximation was applied to compute the thermal expansion coefficient and Grüneisen constant G [58]. The internal energy-volume equation of state provided by Mayer *et al* [59] was used to find the Grüneisen constant G

$$E(v) = \frac{BV_0}{\frac{5}{6} - \gamma_G}\left(\frac{V}{V_0}\right)^{\frac{5}{6}-\gamma_G}\left(\ln\frac{V}{V_0} - \frac{1}{\frac{5}{6} - \gamma_G}\right) + E_\infty, \tag{2}$$

where V_0 is equilibrium volume and B is bulk modulus.

After calculating the γ_G, Debye temperature is calculated as,

$$\theta_D = \frac{\hbar}{K_B}\left(\frac{6\pi^2 q}{V_0}\right)^{\frac{1}{3}} V_m, \tag{3}$$

where V_0 is volume, q represents atoms in the unit cell, $\hbar$, and K_B are Planks and Boltzmann constant, respectively. The specific heat capacity, C_V, as a function of temperature, T, is estimated as,

$$C_{v(T)} = 9qk_B\left(\frac{T}{\theta_D}\right)^3 \int_{x_D}^{0} \frac{x^4 \exp x}{(\exp x - 1)^2} dx \tag{4}$$

where $x_D = \frac{\theta_D}{T}$ and θ_D is a linear thermal expansion coefficient. The linear thermal expansion coefficient (α) is calculated as,

$$\alpha_L(T) = \frac{1}{3}\gamma_G \frac{C_V(T)}{BV_0} \tag{5}$$

3. Results and discussion

3.1. Structural properties

Various parameter calculations were performed which can predict the phase of RHEAs. The entropy of mixing ($\Delta Smix$) [60], enthalpy of mixing ($\Delta Hmix$) [61], unitless parameter (Ω) [62], atomic size difference (δ), and valence electron concentration (VEC) [63] of the alloys, were calculated by the following formula:

$$\Delta S_{mix} = -R\sum_{i=1}^{n} x_i \ln x_i \tag{6}$$

$$\Delta H_{mix} = \sum_{i=1, i\neq j}^{n} 4\Delta H_{ij}^{mix} x_i x_j \tag{7}$$

$$\delta = 100 \times \sqrt{\sum_{i=1}^{n} x_i\left(1 - \frac{r_i}{\bar{r}}\right)^2}\ \bar{r} = \sum_{i=1}^{n} x_i r_i \tag{8}$$

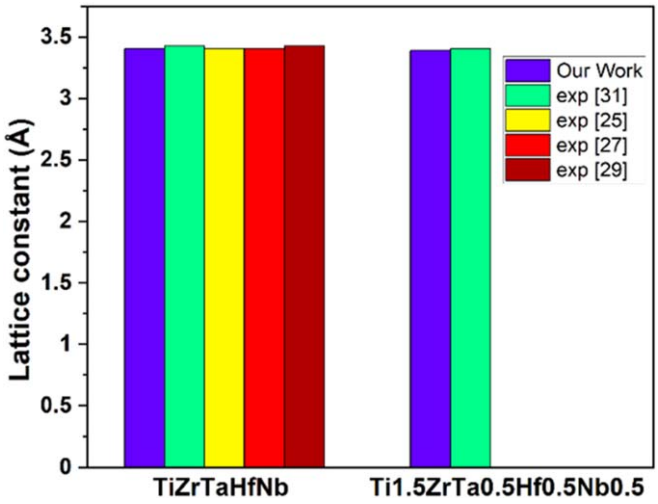

Figure 2. Comparison of calculated lattice constant of HfNbTaTiZr and $Hf_{0.5}Nb_{0.5}Ta_{0.5}Ti_{1.5}Zr$ with available experimental data.

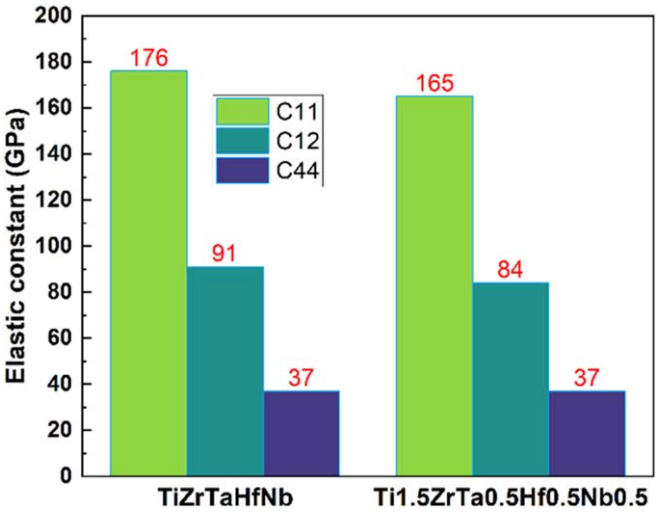

Figure 3. Calculated elastic constant of HfNbTaTiZr and $Hf_{0.5}Nb_{0.5}Ta_{0.5}Ti_{1.5}Zr$ from 100-atom supercell simulation.

Table 1. The calculated parameter ΔSmi_x, ΔHmi_x, VEC, Ω, δ, and T_m of RHEAs.

Name of alloys	ΔS_{mix}(J Kmol^{-1})	$\Delta Hmix$ (KJ mol^{-1})	VEC	Ω	δ	T_m (K)
HfNbTaTiZr	13.38	2.72	4.40	12.41	4.9	2523
$Hf_{0.5}Nb_{0.5}Ta_{0.5}Ti_{1.5}Zr$	12.41	1.84	4.24	15.63	4.63	2322

$$VEC = \sum_{i=1}^{n} x_i (VEC)_i \tag{9}$$

$$\Omega = \frac{T_m \Delta S_{mix}}{|\Delta H_{mix}|},\ T_m = x_i\ (T_m)_i \tag{10}$$

where R is ideal gas constant; x_i *and* x_j are the atomic percentages of the ith and jth element, respectively; r_i is the radius of the ith element; $\bar{r}$ is averaged atomic radius; and $(VEC)_i$ is the valence electron concentration of ith element.

From the report of Zhang *et al* [61] and Sheng *et al* [64], the required conditions for HEAs to form a solid stable solution are: $11 \leqslant \Delta Smix \leqslant 19.5$ (J/K.mol), $-22 \leqslant \Delta Hmix \leqslant 7$ (kJ mol^{-1}), and $\Omega > 1.1$ and $\delta < 6.6\%$. The calculated parameters are shown in table 1, which suggest that two current RHEAs will form a solid solution structure as it satisfies the conditions proposed by references [61, 62]. According to Guo *et al* [63], if the calculated VEC of alloy is lower than 6.67, it will form a BCC crystal structure and both RHEAs have $VEC < 6.67$

Table 2. Calculated ρ (g cm^{-3}), B (GPa), G (GPa), E (GPa), H_v (GPa) and their comparisons with the available experiments.

Name of alloy	ρ	B	G	E	H_v	ν	B/G
HfNbTaTiZr (this work)	9.96	119	35	97	2.92	0.36	3.35
Exp. [33]	9.94 [29]	134 [32]	42 [29]	112.74 ± 4.66	3.14 ± 0.12	0.40 [32]	
	9.92 [32]		38.5 [71]	97.9 ± 6.9 [71]			
$Hf_{0.5}Nb_{0.5}Ta_{0.5}Ti_{1.5}Zr$ (this work)	8.26	111	31	86	2.49	0.37	3.56
Exp. [33]				98.57 ± 4.18	3.02 ± 0.11		

indicating the existence of BCC phase in them. The experimental reports [27, 29, 31, 33] show only BCC phase exists for both RHEAs, which confirms the *VEC* could be the indicative parameter to identify the phase in alloys.

The lattice constant of both RHEAs was calculated using the relaxed super cell volume and results were compared with available experiment data which is shown in figure 2. The calculated lattice constant of HfNbTaTiZr is 3.403 Å which is equal to the experimental values of 3.40 Å [27, 29] and 3.405 Å [31]. Similarly, the calculated lattice constant of $Hf_{0.5}Nb_{0.5}Ta_{0.5}Ti_{1.5}Zr$ was equal to 3.391 and its experimental value is 3.405 [33]. It is seen that the changes in the atomic concentration of alloys from equimolar to non-equimolar lowers the atomic size of alloys as shown in table 1. This lowering of atomic size is responsible for lattice contraction which slightly decrease the lattice constant of $Hf_{0.5}Nb_{0.5}Ta_{0.5}Ti_{1.5}Zr$ [65].

3.2. Mechanical properties

To explore the mechanical properties of two RHEAs, we obtained the elastic constants which are important parameters in determining the stability of materials and calculated values are shown in figure 3. According to the Born Rule, the mechanical stability criteria required for materials are $C_{11} + 2C_{12} > 0$, $C_{11} - C_{12} > 0$, $C_{44}>0$, and $C_{11} > |C_{12}|$. The values of the elastic constants C_{11}, C_{12}, and C_{44} meet the Born stability criteria for both RHEAs, showing that their crystal structures are mechanically stable. The experiment conducted by Dirras *et al* [32] found the C_{11} and C_{44} of HfNbTaTiZr are 172 ± 6 GPa and 28 ± 1.5 GPa, respectively, which is closer to our simulation value. Similarly, Fazakas *et al* [66] calculated the value of C_{11} and C_{44} of HfNbTaTiZr by first-principles method, which are 160 GPa and 62.4 GPa, respectively. The first-principles calculations overestimate the C_{44} value and underestimate the value of C_{11}. The elastic constants C_{11} and C_{12} of HfNbTaTiZr are larger than $Hf_{0.5}Nb_{0.5}Ta_{0.5}Ti_{1.5}Zr$. The reason for higher elastic constant of HfNbTaTiZr could be the lattice distortion brought by size difference in atomic radii of elements [67]. However, there is no significant changes in the C_{44} value for both alloys and the existing first-principles method is not able to provide a conclusive explanation. The Cauchy pressure (C_{11}–C_{44}) of materials is useful in predicting the nature of bonding which, if positive, is likely to form a metallic bond with ductile behaviors [68]. It is found that the value of Cauchy pressure for both alloys are positive which indicates the formation of metallic bonds exists in them and they are ductile in nature. The anisotropy factor (A) [69] is an excellent parameter that reveals how much anisotropy a cubic crystal possesses which is calculated by the following equation

$$A = \frac{2C_{44}}{C_{11} - C_{12}} \tag{11}$$

For isotropic crystals, the anisotropy factor must equal one, and any value of A less or more than one relates to the crystal's degree of elastic anisotropy. The calculated A from elastic constants is 0.87 and 0.91 for HfNbTaTiZr and $Hf_{0.5}Nb_{0.5}Ta_{0.5}Ti_{1.5}Zr$ RHEAs, respectively. As a result, one can conclude that $Hf_{0.5}Nb_{0.5}Ta_{0.5}Ti_{1.5}Zr$ is somewhat more anisotropic than HfNbTaTiZr. Furthermore, the higher value of elastic constants C_{11} and C_{12} increases the other mechanical properties like bulk modulus (B), shear modulus (G), Young's modulus (E) and Vickers's hardness (H_v) in HfNbTaTiZr. The theoretically calculated density (ρ), B, G, E and H_v for both RHEAs are shown in table 2. The Tian's *et al* [70] model was used to calculate the Vickers hardness (H_v) as

$$H_v = 0.92 \times K^{1.137} \times G^{0.708} \tag{12}$$

where $K = \frac{G}{B}$.

The hardness of the HfNbTaTiZr was found to be 2.92 GPa, which is higher than the $Hf_{0.5}Nb_{0.5}Ta_{0.5}Ti_{1.5}Zr$. The increased hardness of HfNbTaTiZr could be due to the cocktail effect [72] which can result in unexpected properties changes in metallic alloys. For metallic alloys, the cocktail effect can be achieved by changing the composition and alloying of materials. According to Pugh's rule [73], ductile material will have a B/G ratio >1.75 and brittle material will have B/G < 1.75. The calculated B/G ratio for both RHEAs is greater than 1.75, which suggests that these RHEAs will have a ductile nature. The calculated Young's modulus of $Hf_{0.5}Nb_{0.5}Ta_{0.5}Ti_{1.5}Zr$ is 86 GPa which is lower than the HfNbTaTiZr. Due to the lower elastic modulus,

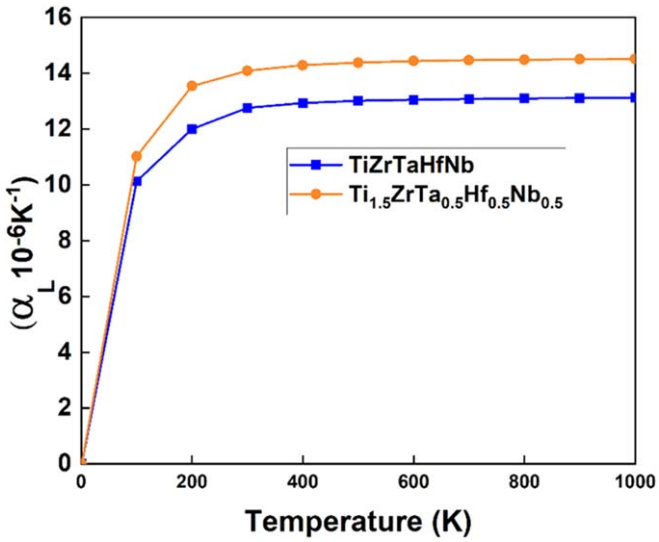

Figure 4. Thermal coefficient of linear expansion (α) as a function of temperature.

$Hf_{0.5}Nb_{0.5}Ta_{0.5}Ti_{1.5}Zr$ could be a potential alloy for bone implants [71]. Furthermore, slightly higher value of poison ratio of $Hf_{0.5}Nb_{0.5}Ta_{0.5}Ti_{1.5}Zr$ indicates its better plastic property [74]. Higher plastic material is easy to handle than brittle material during the manufacturing process. There is a good agreement between the calculated elastic constants, Young's modulus, shear modulus, Poison's ratio (ν), Vickers hardness with the available experimental reports which provides validation of the theoretical analysis. This demonstrates that the random supercell model merged with the DFT-based calculation is a feasible approach to predict the elastic constants and other mechanical properties correctly.

3.3. Thermal properties

It is very necessary to study the thermal stability of alloys at different temperatures in order to use them as a high temperature structural material. Therefore, the thermal properties of both alloys have been studied. Debye temperature (θ_D) has been calculated which helps to identify the natural covalent bond of solid materials. It is found that the material with larger θ_D has a higher chance of forming a strong covalent bond [75]. The calculated θ_D, Grüneisen parameter, and V_m of HfNbTaTiZr are 235.7 K, 2.25, and 2136 m s^{-1}, respectively and those of $Hf_{0.5}Nb_{0.5}Ta_{0.5}Ti_{1.5}Zr$ are 242.9 K, 2.32, and 2205 m s^{-1}. The thermal coefficient of linear expansion (α_L) of two RHEAs is shown in figure 4. It is a very useful parameter for explaining how temperature can change the size of materials and its value has wide application in determining the structural as well as mechanical applications. It can be seen from the diagram that for $Hf_{0.5}Nb_{0.5}Ta_{0.5}Ti_{1.5}Zr$, the α_L value is almost the same as HfNbTaTiZr up to 70 K and becomes higher after 100 K. The higher value of α_L shows its sensitivity nature towards high temperature. Since α_L is inversely proportional to the melting temperature of materials, $Hf_{0.5}Nb_{0.5}Ta_{0.5}Ti_{1.5}Zr$ has a higher melting temperature than HfNbTaTiZr which results in increased α_L as temperature increased. The θ_D and α_L of $Hf_{0.5}Nb_{0.5}Ta_{0.5}Ti_{1.5}Zr$ is greater than the HfNbTaTiZr which implies it has better thermal properties. There is no experimental and theoretical study of thermal properties related to both RHEAs as per the authors' findings. Therefore, simulations of the thermal properties of current RHEAs could provide important guidance for future experimental and *ab-initio* investigation.

It is clear from this computational study that changing the composition of elements of RHEAs could affect the mechanical and thermodynamic properties, often described by four core effects [76]. In this study, various structural, mechanical, and thermal properties of RHEAs have been explored and compared with available experiments. More experimental study is needed to validate some of our computational findings, and it is expected to be confirmed in the near future.

4. Conclusion

The first-principles DFT calculations have been performed to study the structural, mechanical, and thermal properties of two RHEAs, HfNbTaTiZr and $Hf_{0.5}Nb_{0.5}Ta_{0.5}Ti_{1.5}Zr$, with BCC structure. The calculated elastic constants indicate that both RHEAs are mechanically stable. The calculated lattice constant, density, Young's modulus, and hardness for both RHEAs are consistent with the experiments. It is found that the

$Hf_{0.5}Nb_{0.5}Ta_{0.5}Ti_{1.5}Zr$ RHEA have low Young's modulus, high plasticity, and better thermal properties which is likely to be a potential candidate for future biomedical application. The agreement of our computational findings with the available experimental data confirms the efficiency and accuracy of 100 atoms supercell model which is capable of predicting the mechanical properties precisely. Therefore, DFT computational technique could be an alternative cost-effective and efficient method, besides related experiments, to explore the structures, mechanical, and thermodynamical properties of the novel RHEAs that have potential application in biomedical fields.

Acknowledgments

This research was partially supported by the US National Science Foundation (NSF) under grant number OIA-1946231 and the Louisiana Board of Regent for the Louisiana Material Design Alliance (LAMDA), LEQSF-EPS (2021)-LAMDA Seed-Track1B-04/LEQSF-EPS(2021)-LAMDA Seed-Track1A-02, LEQSF-EPS(2020)-SURE-242/LEQSF-EPS(2020)-SURE-237/LEQSF-EPS(2021)-SURE-262. DoE/NNSA award No. DE-NA0003979, and DoD support under contract No. W911NF1910005. The computational work was supported by the Louisiana Optical Network Infrastructure (LONI) with the supercomputer allocation loni_mat_bio15 and 16.

Data availability statement

All data that support the findings of this study are included within the article (and any supplementary files).

ORCID iDs

Feng Gao https://orcid.org/0000-0002-4410-6611
Shengmin Guo https://orcid.org/0000-0002-3673-0836

References

[1] Saini M, Singh Y, Arora P, Arora V and Jain K 2015 Implant biomaterials: a comprehensive review *World Journal of Clinical Cases: WJCC* **3** 52
[2] Zalnezhad E, Hamouda A M S, Faraji G and Shamshirband S 2015 TiO_2 nanotube coating on stainless steel 304 for biomedical applications *Ceram. Int.* **41** 2785–93
[3] Zhu S L, Wang X M, Qin F X and Inoue A 2007 A new Ti-based bulk glassy alloy with potential for biomedical application *Mater. Sci. Eng. A* **459** 233–7
[4] Bai Y, Hao Y L, Li S J, Hao Y Q, Yang R and Prima F 2013 Corrosion behavior of biomedical Ti– 24Nb–4Zr–8Sn alloy in different simulated body solutions *Mater. Sci. Eng. C* **33** 2159–67
[5] Liu S, Liu J, Wang L, Ma R L W, Zhong Y, Lu W and Zhang L C 2020 Superelastic behavior of in- situ eutectic-reaction manufactured high strength 3D porous NiTi-Nb scaffold *Scr. Mater.* **181** 121–6
[6] Wang W, Han P, Peng P, Zhang T, Liu Q, Yuan S N, Huang L Y, Yu H L, Qiao K and Wang K S 2020 Friction stir processing of magnesium alloys: a review *Acta Metallurgica Sinica (English Letters)* **33** 43–57
[7] Zhao G H, Aune R E and Espallargas N 2016 Tribocorrosion studies of metallic biomaterials: the effect of plasma nitriding and DLC surface modifications *J. Mech. Behav. Biomed. Mater.* **63** 100–14
[8] Zhou Z, Wei Q, Li Q, Jiang B, Chen Y and Sun Y 2016 Development of Co-based bulk metallic glasses as potential biomaterials *Mater. Sci. Eng. C* **69** 46–51
[9] Chen Q and Thouas G A 2015 Metallic implant biomaterials *Mater. Sci. Eng. R Rep.* **87** 1–57
[10] Onodera R, Asakawa S, Segawa R, Mizuno N, Ogasawara K, Hiratsuka M and Hirasawa N 2018 Zinc ions have a potential to attenuate both Ni ion uptake and Ni ion-induced inflammation *Sci. Rep.* **8** 1–11
[11] Au A, Ha J, Hernandez M, Polotsky A, Hungerford D S and Frondoza C G 2006 Nickel and vanadium metal ions induce apoptosis of T-lymphocyte Jurkat cells *Journal of Biomedical Materials Research A* **79** 512–21
[12] Geetha M, Singh A K, Asokamani R and Gogia A K 2009 Ti based biomaterials, the ultimate choice for orthopaedic implants—a review *Prog. Mater Sci.* **54** 397–425
[13] Manivasagam G, Dhinasekaran D and Rajamanickam A 2010 Biomedical implants: corrosion and its prevention—a review *Recent Patents on Corrosion Science* (https://doi.org/10.2174/1877610801002010040)
[14] Manam N S, Harun W S W, Shri D N A, Ghani S A C, Kurniawan T, Ismail M H and Ibrahim M H I 2017 Study of corrosion in biocompatible metals for implants: a review *J. Alloys Compd.* **701** 698–715
[15] Kopova I, Stráský J, Harcuba P, Landa M, Janeček M and Bačákova L 2016 Newly developed Ti– Nb–Zr–Ta–Si–Fe biomedical beta titanium alloys with increased strength and enhanced biocompatibility *Mater. Sci. Eng. C* **60** 230–8
[16] Niinomi M, Narushima T and Nakai M 2015 *Advances in Metallic Biomaterials: Tissues, Materials and Biological Reactions* vol 3 (Berlin Heidelberg: Springer)
[17] Wen C 2015 *Surface Coating and Modification for Metallic Biomaterials* (Cambridge: Woodhead)
[18] Eliaz N 2019 Corrosion of metallic biomaterials: a review *Materials* **12** 407
[19] Masahashi N, Mizukoshi Y, Semboshi S, Ohtsu N, Jung T K and Hanada S 2010 Photo-induced characteristics of a Ti–Nb–Sn biometallic alloy with low Young's modulus *Thin Solid Films* **519** 276- 283
[20] Chen J, Zhou X, Wang W, Liu B, Lv Y, Yang W, Xu D and Liu Y 2018 A review on fundamental of high entropy alloys with promising high–temperature properties *J. Alloys Compd.* **760** 15–30

[21] Senkov O N, Miracle D B, Chaput K J and Couzinie J P 2018 Development and exploration of refractory high entropy alloys—a review *J. Mater. Res.* **33** 3092–128
[22] Yang X and Hutchinson C R 2016 Corrosion-wear of β-Ti alloy TMZF (Ti-12Mo-6Zr-2Fe) in simulated body fluid *Acta Biomater.* **42** 429–39
[23] Long M and Rack H J 2005 Subsurface deformation and microcrack formation in Ti–35Nb–8Zr–5Ta–O (x) during reciprocating sliding wear *Mater. Sci. Eng. C* **25** 382–8
[24] De Almeida L H, Bastos I N, Santos I D, Dutra A J B, Nunes C A and Gabriel S B 2014 Corrosion resistance of aged Ti–Mo–Nb alloys for biomedical applications *J. Alloys Compd.* **615** S666–9
[25] Qin F X, Wang X M, Xie G Q and Inoue A 2008 Distinct plastic strain of Ni-free Ti–Zr–Cu–Pd–Nb bulk metallic glasses with potential for biomedical applications *Intermetallics* **16** 1026–30
[26] Yan X and Zhang Y 2020 Functional properties and promising applications of high entropy alloys *Scr. Mater.* **187** 188–93
[27] Stepanov N D, Yurchenko N Y, Zherebtsov S V, Tikhonovsky M A and Salishchev G A 2018 Aging behavior of the HfNbTaTiZr high entropy alloy *Mater. Lett.* **211** 87–90
[28] Senkov O N and Semiatin S L 2015 Microstructure and properties of a refractory high-entropy alloy after cold working *J. Alloys Compd.* **649** 1110–23
[29] Senkov O N, Scott J M, Senkova S V, Miracle D B and Woodward cf 2011 Microstructure and room temperature properties of a high-entropy TaNbHfZrTi alloy *J. Alloys Compd.* **509** 6043–8
[30] Couzinié J P, Lilensten L, Champion Y, Dirras G, Perrière L and Guillot I 2015 On the room temperature deformation mechanisms of a TiZrHfNbTa refractory high-entropy alloy *Mater. Sci. Eng. A* **645** 255–63
[31] Senkov O N, Scott J M, Senkova S V, Meisenkothen F, Miracle D B and Woodward cf 2012 Microstructure and elevated temperature properties of a refractory TaNbHfZrTi alloy *J. Mater. Sci.* **47** 4062–74
[32] Dirras G, Lilensten L, Djemia P, Laurent-Brocq M, Tingaud D, Couzinié J P, Perrière L, Chauveau T and Guillot I 2016 Elastic and plastic properties of as-cast equimolar TiHfZrTaNb high-entropy alloy *Mater. Sci. Eng. A* **654** 30–8
[33] Motallebzadeh A, Peighambardoust N S, Sheikh S, Murakami H, Guo S and Canadinc D 2019 Microstructural, mechanical and electrochemical characterization of TiZrTaHfNb and Ti1. 5ZrTa0. 5Hf0. 5Nb0. 5 refractory high-entropy alloys for biomedical applications *Intermetallics* **113** 106572
[34] Wang S P and Xu J 2017 TiZrNbTaMo high-entropy alloy designed for orthopedic implants: as-cast microstructure and mechanical pro^g(1perties *Mater. Sci. Eng. C* **73** 80–9
[35] Guo Y, Li X and Liu Q 2020 A novel biomedical high-entropy alloy and its laser-clad coating designed by a cluster-plus-glue-atom model *Mater. Des.* **196** 109085
[36] Gurel S, Yagci M B, Canadinc D, Gerstein G, Bal B and Maier H J 2021 Fracture behavior of novel biomedical Ti-based high entropy alloys under impact loading *Mater. Sci. Eng. A* **803** 140456
[37] Nagase T, Iijima Y, Matsugaki A, Ameyama K and Nakano T 2020 Design and fabrication of Ti–Zr- Hf-Cr-Mo and Ti–Zr-Hf-Co-Cr-Mo high-entropy alloys as metallic biomaterials *Mater. Sci. Eng. C* **107** 110322
[38] Hua N, Wang W, Wang Q, Ye Y, Lin S, Zhang L, Guo Q, Brechtl J and Liaw P K 2021 Mechanical, corrosion, and wear properties of biomedical Ti–Zr–Nb–Ta–Mo high entropy alloys *J. Alloys Compd.* **861** 157997
[39] Gurel S, Yagci M B, Bal B and Canadinc D 2020 Corrosion behavior of novel titanium-based high entropy alloys designed for medical implants *Mater. Chem. Phys.* **254** 123377
[40] Iijima Y, Nagase T, Matsugaki A, Wang P, Ameyama K and Nakano T 2021 Design and development of Ti–Zr–Hf–Nb–Ta–Mo high-entropy alloys for metallic biomaterials *Mater. Des.* **202** 09548
[41] Kresse G and Furthmüller J 1996 Efficient iterative schemes for ab initio total-energy calculations using a plane-wave basis set *Physical review B* **54** 11169
[42] MedeA® Software. Available online: (https://materialsdesign.com/medea-software)(accessed on 19 May 2021)
[43] Perdew J P, Burke K and Ernzerhof M 1996 Generalized gradient approximation made simple *Phys. Rev. Lett.* **77** 3865
[44] Monkhorst H J and Pack J D 1976 Special points for Brillouin-zone integrations *Physical Review B* **13** 5188
[45] Hu J, Zhang J, Xiao H, Xie L, Shen H, Li P, Zhang J, Gong H and Zu X 2020 A density functional theory study of the hydrogen absorption in high entropy alloy TiZrHfMoNb *Inorg. Chem.* **59** 9774–82
[46] Hu J, Zhang J, Xiao H, Xie L, Sun G, Shen H, Li P, Zhang J and Zu X 2021 The effect of hydrogen on the mechanical properties of high entropy alloy TiZrHfMoNb: First-principles investigation *J. Alloys Compd.* **879** 160482
[47] Chen L, Zhang X, Wang Y, Hao X and Liu H 2019 Microstructure and elastic constants of AlTiVMoNb refractory high-entropy alloy coating on Ti6Al4V by laser cladding *Mater. Res. Express* **6** 116571
[48] Chen L, Hao X, Wang Y, Zhang X and Liu H 2020 First-principles calculation of the effect of Ti content on the structure and properties of TiVNbMo refractory high-entropy alloy *Mater. Res. Express* **7** 106516
[49] Knuth E D 1965 *The Art of Computer Programming* (Massachusett: Addison-Wesley)
[50] Bellaiche L and Vanderbilt D 2000 Virtual crystal approximation revisited: application to dielectric and piezoelectric properties of perovskites *Physical Review B* **61** 7877–82
[51] Zunger A, Wei S H, Ferreira L G and Bernard J E 1990 Special quasirandom structures *Phys. Rev. Lett.* **65** 353–6
[52] Wang S, Xiong J, Li D, Zeng Q, Xiong M and Chai X 2021 Comparison of two calculation models for high entropy alloys: virtual crystal approximation and special quasi-random structure *Mater. Lett.* **282** 28754
[53] Tian L Y, Wang G, Harris J S, Irving D L, Zhao J and Vitos L 2017 Alloying effect on the elastic properties of refractory high-entropy alloys *Mater. Des.* **114** 243–52
[54] Bhandari U, Zhang C and Yang S 2020 Mechanical and thermal properties of low-density Al20 + xCr20- xMo20-yTi20V20+y Alloys *Crystals* **10** 278
[55] Le Page Y and Saxe P 2001 Symmetry-general least-squares extraction of elastic coefficients from ab initio total energy calculations *Physical Review B* **63** 174103
[56] Le Page Y and Saxe P 2002 Symmetry-general least-squares extraction of elastic data for strained materials from ab initio calculations of stress *Physical Review B* **65** 104104
[57] Zuo L I, Humbert M I and Esling C L 1992 Elastic properties of polycrystals in the voigt-reuss-hill approximation *J. Appl. Crystallogr.* **25** 751–5
[58] Anderson O L 1963 A simplified method for calculating the debye temperature from elastic constants *J. Phys. Chem. Solids* **24** 909–17
[59] Mayer B, Anton H, Bott E, Methfessel M, Sticht J, Harris J and Schmidt P C 2003 *Ab-initio* calculation of the elastic constants and thermal expansion coefficients of laves phases *Intermetallics* **11** 23–32

[60] Zhang Y, Zhou Y J, Lin J P, Chen G L and Liaw P K 2008 Solid-solution phase formation rules for multi-component alloys *Adv. Eng. Mater.* **10** 534–8
[61] Takeuchi A and Inoue A 2005 Classification of bulk metallic glasses by atomic size difference, heat of mixing and period of constituent elements and its application to characterization of the main alloying element *Mater. Trans.* **46** 2817–29
[62] Zhang Y, Zuo T T, Tang Z, Gao M C, Dahmen K A, Liaw P K and Lu Z P 2014 Microstructures and properties of high-entropy alloys *Prog. Mater Sci.* **61** 1–93
[63] Guo S, Ng C, Lu J and Liu C T 2011 Effect of valence electron concentration on stability of fcc or bcc phase in high entropy alloys *J. Appl. Phys.* **109** 103505
[64] Sheng G U O and Liu C T 2011 Phase stability in high entropy alloys: formation of solid-solution phase or amorphous phase *Progress in Natural Science: Materials International* **21** 433–46
[65] Du Z, Zuo J, Bao N, Yang M, Jiang G and Zhang L 2019 Effect of Ta addition on the structural, thermodynamic and mechanical properties of CoCrFeNi high entropy alloys *RSC Adv.* **9** 16447–54
[66] Fazakas E, Zadorozhnyy V, Varga L K, Inoue A, Louzguine-Luzgin D V, Tian F and Vitos L 2014 Experimental and theoretical study of Ti20Zr20Hf20Nb20X20 (X = V or Cr) refractory high-entropy alloys *Int. J. Refract. Met. Hard Mater* **47** 131–8
[67] Yeh J W, Lin S J, Chin T S, Gan J Y, Chen S K, Shun T T, Tsau C H and Chou S Y 2004 Formation of simple crystal structures in Cu–Co–Ni–Cr–Al–Fe–Ti–V alloys with multiprincipal metallic elements *Metallurgical and Materials Transactions A* **35** 2533–6
[68] Pettifor D G 1992 Theoretical predictions of structure and related properties of intermetallics *Mater. Sci. Technol.* **8** 345–9
[69] Chung D H and Buessem W R 1967 The elastic anisotropy of crystals *J. Appl. Phys.* **38** 2010–2
[70] Tian Y, Xu B and Zhao Z 2012 Microscopic theory of hardness and design of novel superhard crystals *Int. J. Refract. Met. Hard Mater* **33** 93–106
[71] Senkov O N, Pilchak A L and Semiatin S L 2018 Effect of cold deformation and annealing on the microstructure and tensile properties of a HfNbTaTiZr refractory high entropy alloy *Metallurgical and Materials Transactions A* **49** 2876–92
[72] Yeh J W 2015 Physical metallurgy of high-entropy alloys *JOM* **67** 2254–61
[73] Pugh S F 1954 XCII. Relations between the elastic moduli and the plastic properties of polycrystalline pure metals *The London, Edinburgh, and Dublin Philosophical Magazine and Journal of Science* **45** 823- 843
[74] Liu Y, Wang K, Xiao H, Chen G, Wang Z, Hu T, Fan T and Ma L 2020 Theoretical study of the mechanical properties of CrFeCoNiMo x ($0.1 \leqslant x \leqslant 0.3$) alloys *RSC Adv.* **10** 14080–8
[75] Wang S, Zhao Y, Hou H, Wen Z, Zhang P and Liang J 2018 Effect of anti-site point defects on the mechanical and thermodynamic properties of $MgZn_2$, $MgCu_2$ Laves phases: a first-principle study *J. Solid State Chem.* **263** 18–23
[76] Cantor B, Chang I T H, Knight P and Vincent A J B 2004 Microstructural development in equiatomic multicomponent alloys *Mater. Sci. Eng. A* **375** 213–8